Synchronization in a carpet of hydrodynamically coupled rotors with random intrinsic frequency

A Letters Journal Exploring the Frontiers of Physics

March 2010

EPL, **89** (2010) 50011
doi: 10.1209/0295-5075/89/50011

www.epljournal.org

Synchronization in a carpet of hydrodynamically coupled rotors with random intrinsic frequency

N. Uchida[1(a)] and R. Golestanian[2]

[1] *Department of Physics, Tohoku University - Sendai, 980-8578, Japan*
[2] *Department of Physics and Astronomy, University of Sheffield - Sheffield S3 7RH, UK, EU*

received 15 Janaury 2010; accepted in final form 1 March 2010
published online 26 March 2010

PACS 05.45.Xt – Synchronization; coupled oscillators
PACS 87.19.rh – Fluid transport and rheology
PACS 07.10.cm – Micromechanical devices and systems

Abstract – We investigate synchronization caused by long-range hydrodynamic interaction in a two-dimensional, substrated array of rotors with random intrinsic frequencies. The rotor mimics a flagellated bacterium that is attached to the substrate ("bacterial carpet") and exerts an active force on the fluid. Transition from coherent to incoherent regimes is studied numerically, and the results are compared to a mean-field theory. We show that quite a narrow distribution of the intrinsic frequency is required to achieve collective motion in realistic cases. The transition is gradual, and the critical behavior is qualitatively different from that of the conventional globally coupled oscillators. The model not only serves as a novel example of non-locally coupled oscillators, but also provides insights into the role of intrinsic heterogeneities in living and artificial microfluidic actuators.

Introduction. – Collective oscillations of active elements are observed in a variety of physical, chemical, and biological systems far from equilibrium. Numerous studies have been devoted to the mutual entrainment of oscillators that have different intrinsic frequencies [1,2]. A class of phase oscillators with global (or mean-field) coupling have enjoyed deep theoretical understanding [1–3], while a myriad of unresolved problems still remain on the behaviors of locally [4] and non-locally [5,6] coupled oscillators. In particular, knowledge about synchronization caused by long-range interactions is quite limited [7–9], although they are ubiquitous in Nature in the form of, *e.g.*, gravitational, electromagnetic, elastic, and hydrodynamic forces.

Biologically important examples of long-ranged synchronization are provided by swimming microorganisms that are interacting hydrodynamically, such as sperm flagella beating in harmony [10–14], and metachronal waves in cilia [15–19]. Both of these oscillatory elements, flagella and cilia, are driven by molecular motors embedded in the cell surface, and interact through the viscous environment (water). In order to describe their synchronized motion, several theoretical models have been proposed [10,12,13,15–19]. While all of these initial studies are focused on a homogeneous set of identical systems, it will be important to consider the role of disorder, as real biological motors possess intrinsic heterogeneities that could affect the collective dynamics.

An example of collective yet heterogeneous dynamics is found in a bacterial carpet, which is recently introduced as a new type of microfluidic device [20]. The assembly is composed of a dense monolayer of bacteria that are lightly attached to a solid substrate by their bodies (heads). The bacteria have partial freedom to reorient their flagella (tails), which pump the fluid and are orientationally ordered by hydrodynamic interaction. Evolution of correlated regions is observed, but the ordering remains partial. Observations of irregular and slowly varying flow structures ("whirlpools" and "rivers") suggest the presence of heterogeneity in the configurations of the rotors [21]. Fabrication of more efficient microfluidic pumps could be achieved through understanding and controlling the heterogeneity.

Recently, we have proposed a generic model of hydrodynamically coupled rotors arrayed on a substrate, and studied the collective dynamics of uniform elements [22]. In this letter, using a variant of the model, we address the

(a) E-mail: uchida@cmpt.phys.tohoku.ac.jp

effect of random intrinsic frequencies on synchronization. To be concrete, we consider a simple and idealized model of bacterial carpets. We assume that the bacteria have complete freedom to reorient their flagellar tails without any torque supported by the substrate. This is modeled by mounting each flagellated bacterium on the tip of a freely rotatable arm stemming from the substrate. In a real bacterial carpet, there is no such arm, but the flagellum is located at finite distance and height from the point where the body is attached to the substrate (around which the bacterium can partially rotate); see fig. 1(a). These lengths are in the order of the diameter of the body, and correspond to the length and height of the arm in our model. We assume that the mounting angle of the flagellum relative to the arm varies from one rotor to another, while the magnitude of the force generated is assumed to be constant and uniform. Depending on the sign of the mounting angle, the flagellum generates a torque that drives the rotor in either clockwise or counterclockwise direction. We assume that the mounting angle and hence the intrinsic frequency of the rotor are randomly distributed around zero. By varying the degree of randomness, we study the transition from coherent to incoherent regimes numerically. Our results suggest that synchronization of the rotors, and hence collective pumping of the fluid, require a quite narrow distribution of the mounting angle in realistic cases. In order to understand the transition behavior, we apply the mean-field theory, which is originally developed for global coupling, to our long-ranged system. While we obtain a fair agreement between theory and simulation for the synchronization threshold, the transition is shown to be more gradual than in globally coupled oscillators.

Model. – We consider an array of rotors positioned on a square lattice of grid size d. Each rotor has a thin, freely-rotatable arm on the tip of which a flagellated bacterium is mounted. The flagellum consists of a spherical bead of radius a (body) and a thin tail that lies horizontally (flagellum). Motion of the bead is constrained on a circular orbit of radius b located at height h from the substrate, which we take to be the xy-plane. The position of the i-th bead is thus given by $\mathbf{r}_i = \mathbf{r}_{0i} + h\boldsymbol{e}_z + b\boldsymbol{n}_i$ where $\mathbf{r}_{0i}$ is its base position on the square lattice and $\boldsymbol{n}_i = (\cos\phi_i, \sin\phi_i, 0)$ is the unit vector that gives the orientation of the arm via its phase $\phi_i = \phi_i(t)$. The velocity of the bead reads $\mathbf{v}_i = \dot{\phi}_i \boldsymbol{t}_i$, where $\boldsymbol{t}_i = (-\sin\phi_i, \cos\phi_i, 0)$ is the unit vector tangential to the trajectory. We assume that the active force $\boldsymbol{F}_i$ exerted by the rotor on the fluid has a constant magnitude F, and makes a fixed angle δ_i (measured clockwise) from the radial direction; $\boldsymbol{F}_i = F(\cos\delta_i \boldsymbol{n}_i - \sin\delta_i \boldsymbol{t}_i)$. See fig. 1(b) for the configuration. The reaction force $-\boldsymbol{F}_i$ on the rotor arm gives the driving torque $T_i = Fb\sin\delta_i$ and the intrinsic frequency $\omega_i = F\sin\delta_i/\zeta b$, where $\zeta = 6\pi\eta a$ is the viscous drag coefficient. The mounting angles δ_i's are assumed to have the

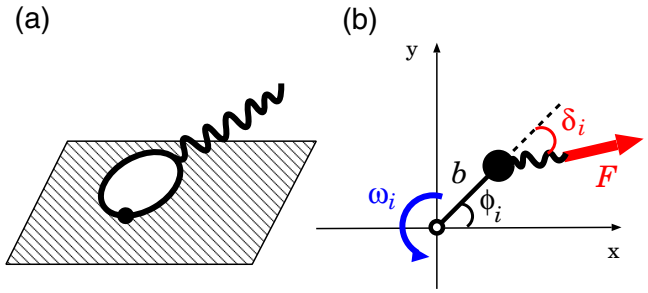

Fig. 1: (Colour on-line) Schematic pictures of a) a bacterium in real bacterial carpet, and (b) the rotor in our model (top view). In (a), the bacterium can partially rotate around the point of attachment to the substrate (black dot). In (b), the active force $\boldsymbol{F}_i$ exerted by the i-th rotor on the fluid is deviated by a fixed angle δ_i from the radial direction. The reaction force drives the rotor at the intrinsic frequency $\omega_i = F\sin\delta_i/\zeta b$, where b is the radius of rotation and ζ the viscous drag coefficient of the bead.

Gaussian distribution

$$P(\delta) = \frac{1}{\sqrt{2\pi}\delta_0} \exp\left(-\frac{\delta^2}{2\delta_0^2}\right) \tag{1}$$

with the standard deviation δ_0.

We assume that the rotors are widely spaced so that $a, b, h \ll d$. Then the velocity field of the fluid created by the active forces is given by $\mathbf{v}(\mathbf{r}) = \sum_i \mathbf{G}(\mathbf{r} - \mathbf{r}_i)\cdot\boldsymbol{F}_i$, where $\mathbf{G}(\mathbf{r}) = (3h^2/2\pi\eta)\cdot\mathbf{r}_\perp\mathbf{r}_\perp/|\mathbf{r}_\perp|^5$, $\mathbf{r}_\perp = (x, y, 0)$ is the asymptotic expression of the Oseen-Blake tensor [23] for $h/d \ll 1$. The rotor's angular velocity is given by $\omega_i + \mathbf{v}(\mathbf{r}_i)\cdot\boldsymbol{t}_i/b$, or, more explicitly,

$$\frac{\mathrm{d}\phi_i}{\mathrm{d}t} = \omega_0 \sin\delta_i - \frac{3\gamma\omega_0 d^3}{4\pi} \sum_{j\neq i} \frac{1}{|\mathbf{r}_{ij}|^3} [\sin(\phi_i - \phi_j + \delta_j) + \cos(\phi_i + \phi_j - \delta_j - 2\theta_{ij})] . \tag{2}$$

Here, $\omega_0 = F/\zeta b$, $\mathbf{r}_{ij} = \mathbf{r}_i - \mathbf{r}_j = |\mathbf{r}_{ij}|(\cos\theta_{ij}, \sin\theta_{ij})$, and $\gamma = \zeta h^2/\eta d^3 = 6\pi a h^2/d^3$ is the dimensionless coupling constant. For a real bacterial carpet, $a \sim h \sim 1\,\mu$m and $d \sim 10\,\mu$m give the rough estimate $\gamma \sim 10^{-2}$.

Numerical simulation. – We implemented the model on a $L \times L$ square lattice and numerically integrated eq. (2) by the Euler method. We assumed the periodic boundary condition and computed the velocity field every time step in the Fourier space. We set $\gamma = 0.1$ and varied the angle deviation δ_0 as the control parameter. The system size used was $L = 128$ for most of the results shown below, while $L = 32$, 64 and 256 are also used to check finite-size effect. Starting from random initial configurations of $\phi_i(t = 0)$, the system reached a dynamical steady state by the time $t = 1 \times 10^4/\omega_0$. The initial transient stage is characterized by coarsening of topological defects for small δ_0, the structure and dynamics of which are discussed elsewhere [22]. In the present paper, we shall

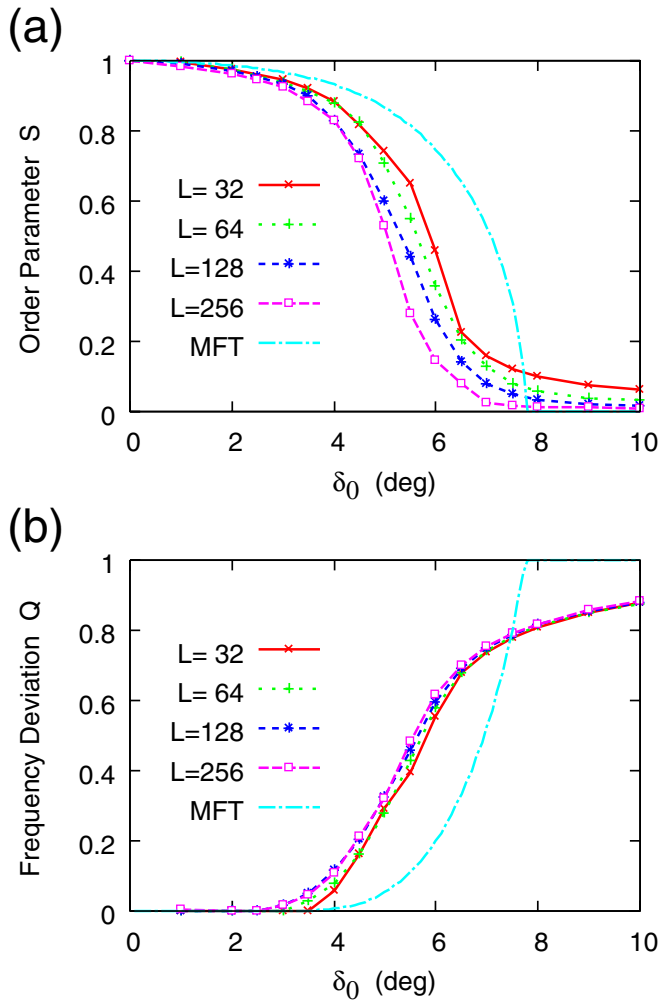

Fig. 2: (Colour on-line) Transition behavior for system size $L = 32, 64, 128$, and 256 with comparison to the mean-field theory (MFT). (a) Orientational order parameter $S = |\langle \boldsymbol{n} \rangle| = |\langle e^{i\phi} \rangle|$ *vs.* δ_0. (b) Normalized frequency deviation $Q = \sqrt{\langle \Omega^2 \rangle / \langle \omega^2 \rangle}$ *vs.* δ_0.

focus on statistical properties of the dynamical steady states. The statistical data shown below are taken from the time window $1 \times 10^4 < \omega_0 t < 2.5 \times 10^5$.

We plot the orientational order parameter $S = |\langle \boldsymbol{n} \rangle| = |\langle e^{i\phi} \rangle|$ as a function of δ_0 in fig. 2. Also shown is the standard deviation (STD) of the actual frequency $\Omega_i = \langle \dot{\phi}_i \rangle_t$ normalized by the STD of the intrinsic frequency ω_i, $Q = \sqrt{\langle \Omega^2 \rangle / \langle \omega^2 \rangle}$. Here and hereafter, the simple angular brackets $\langle \cdots \rangle$ mean the average over both site and time unless otherwise stated, while $\langle \cdots \rangle_{\mathbf{r}}$ and $\langle \cdots \rangle_t$ mean the site-average and time-average, respectively. Note that $S = 1$ and $Q = 0$ in the fully synchronized state and $S = 0$ and $Q = 1$ in the desynchronized limit. As we increase δ_0, S and Q slowly converge to the desynchronized limit. While the change in the orientational order parameter is sharper for a larger system size, the frequency deviation has little L-dependence. For comparison, we also show the results of the mean-field theory, which will be explained in the next section.

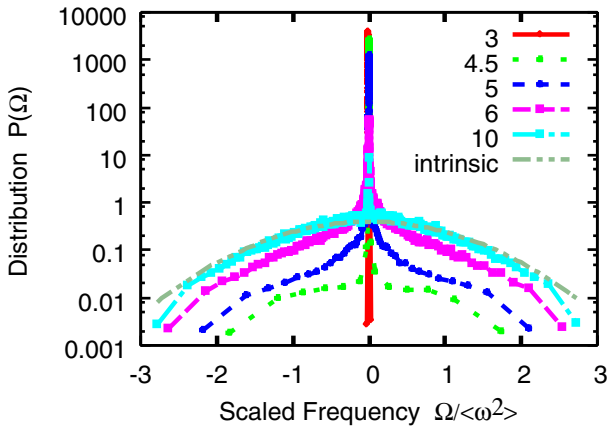

Fig. 3: (Colour on-line) Distribution of the normalized actual frequency $\Omega/\sqrt{\langle \omega^2 \rangle}$ as functions of δ_0. For comparison, the distribution of the intrinsic frequency ω_i is also shown.

In fig. 3, we plot the distribution function of the actual frequency Ω normalized by the STD of intrinsic frequency, for different values of δ_0. The distribution consists of a sharp delta-function like peak at $\Omega = 0$ and broad symmetric tails for $\Omega > 0$ and $\Omega < 0$. For $\delta_0 \leqslant 3°$, most of the rotors are coherent and contribute to the center-peak. For $\delta_0 = 10°$, the distribution is close to that of the intrinsic frequency, while the center peak still remains. the above data suggest that the synchronization transition in this system is more gradual than that found in a globally coupled system, and it is difficult to locate the transition point exactly.

Next we plot the time series of the order parameter $S(t) = |\langle \boldsymbol{n}(t) \rangle_{\mathbf{r}}|$ in fig. 4(a) and its variance $\mathrm{Var}(S) = \langle S(t)^2 \rangle_t - \langle S(t) \rangle_t^2$ as a function of δ_0 in fig. 4(b). The variance has a peak near $\delta_0 = 6°$, suggesting that there is a subtle balance between synchronization and desynchronization. We will call this the threshold angle and denote by δ_{th}. In fig. 4(c), we plot the temporal correlation function of the order parameter $C_S(t) = \langle S(t+t')S(t') \rangle_{t'} - \langle S(t) \rangle_t^2$. We find an oscillatory behavior with long correlation time at $\delta_0 = \delta_{th} = 6°$. Although the origin of the oscillation is beyond the scope of the present paper, a preliminary study shows that the oscillatory behavior at the threshold angle is a unique feature resulting from the long-ranged nature of the interaction.

In fig. 5, we plot the orientational correlation function

$$G_n(|\mathbf{r}|) = \langle [\boldsymbol{n}(\mathbf{r}+\mathbf{r}') - \langle \boldsymbol{n} \rangle] \cdot [\boldsymbol{n}(\mathbf{r}') - \langle \boldsymbol{n} \rangle] \rangle_{\mathbf{r}'}. \qquad (3)$$

Here the outer angular brackets mean taking average over $\mathbf{r}'$ as well as the azimuthal angle of $\mathbf{r}$. For $4 \leqslant \delta_0 \leqslant 6°$, we observe an exponential decay of the correlation over a wide distance. For $\delta_0 > 6°$, on the other hand, the correlation is short-ranged and decays more slowly than exponential. The qualitative change in the correlation function gives

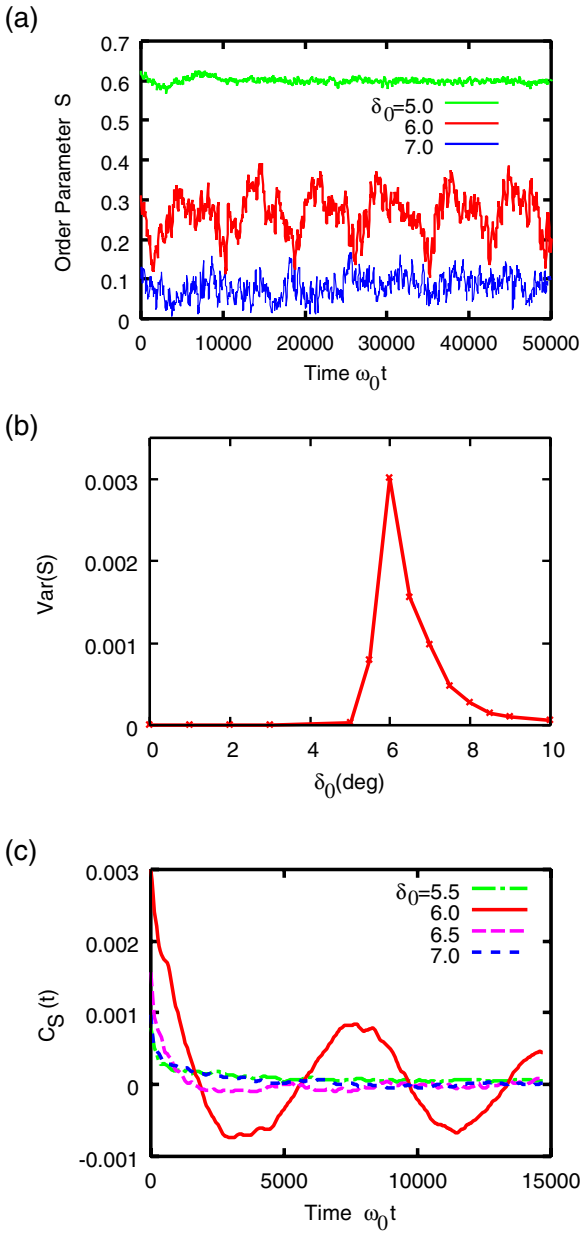

Fig. 4: (Colour on-line) (a) Time series of the order parameter $S(t)$. (b) Variance of the order parameter $\mathrm{Var}(S)$ as a function of δ_0. Fluctuation is most enhanced at $\delta_0 = 6°$. (c) Auto-correlation function of the order parameter $C_S(t)$. An oscillatory behavior is prominent at $\delta_0 = 6°$.

another support of the above estimate of the threshold angle.

Mean-field theory. – In this section, we compare the numerical results with a mean-field theory for a simplifided version of our model. First, when the coupling is weak ($\gamma \ll 1$) and the force angle is small ($\delta_0 \ll 1$), we can neglect the δ_j's in the RHS of eq. (2) because they give $O(\gamma\delta_0)$ contributions. Next, as a part of our mean-field ansatz, we replace the interaction kernel $\propto \mathbf{r}_\perp\mathbf{r}_\perp/r_\perp^5$ by its angular average, as a result of which the cosine term in

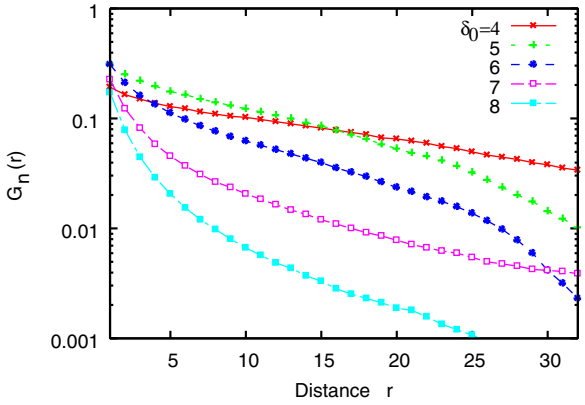

Fig. 5: (Colour on-line) Orientational correlation function $G_n(r)$. Nearly exponential decay of correlation is observed for $\delta_0 \leqslant 6°$.

the RHS of eq. (2) is dropped. It gives the phase equation in the familiar form,

$$\frac{\mathrm{d}\phi_i}{\mathrm{d}t} = \omega_i - \sum_{j\neq i} G(\mathbf{r}_i - \mathbf{r}_j)\sin(\phi_i - \phi_j) \tag{4}$$

with $\omega_i = \omega_0 \sin\delta_i$ and $G(\mathbf{r}) = 3\gamma\omega_0 d^3/4\pi r^3$. The distribution of the intrinsic frequency is given by $P_\omega(\omega) = |\mathrm{d}\delta/\mathrm{d}\omega|P(\delta) = P(\sin^{-1}(\omega/\omega_0))/\sqrt{\omega_0^2 - \omega^2}$.

Now we apply the mean-field ansatz which was originally proposed by Kuramoto [1] for global coupling:

$$Re^{i\theta} = \sum_j G(\mathbf{r}_i - \mathbf{r}_j)e^{i\phi_j}. \tag{5}$$

Here, the amplitude R and the phase θ of the order parameter are assumed to be constant in space and time, which would be justified if the interaction is sufficiently long-ranged. The isotropy of $G(\mathbf{r})$ allows us to assume $\theta = 0$ without loss of generality. Using this we can rewrite eq. (4) as

$$\frac{\mathrm{d}\phi_i}{\mathrm{d}t} = \omega_i - R\sin\phi_i. \tag{6}$$

Equation (6) allows a stationary ($\dot{\phi} = 0$) solution if and only if $|\omega_i| < R$. The rotors satisfying this condition have the actual frequency $\Omega = 0$ and are called the coherent group. The phase of a rotor belonging to this group is given by

$$\phi_i = \sin^{-1}\left(\frac{\omega_i}{R}\right). \tag{7}$$

where the principal value of the inverse-sine function should be chosen so that $|\phi| < \pi/2$. The phase distribution $n(\phi)$ of the coherent group reads

$$n(\phi) = P_\omega(\omega)\cdot\left|\frac{\mathrm{d}\omega}{\mathrm{d}\phi}\right| = P_\omega(R\sin\phi)\cdot R\cos\phi. \tag{8}$$

The rotors with $|\omega(\mathbf{r})| > R$, on the other hand, form the incoherent group. The actual frequency of a rotor belonging to this group is given by

$$\Omega_i = \frac{2\pi}{\int_0^{2\pi} \mathrm{d}\phi \frac{\mathrm{d}t}{\mathrm{d}\phi}} = \sqrt{\omega_i^2 - R^2}. \tag{9}$$

The phase distribution $n'(\phi) = n'(\phi;\omega_i)$ of an incoherent rotor is proportional to the frequency it comes to ϕ:

$$n'(\phi;\omega_i) = C|\dot{\phi}|^{-1} = C|\omega_i - R\sin\phi|^{-1} \tag{10}$$

with the normalization factor $C = \sqrt{\omega_i^2 - R^2}/2\pi$.

Now we replace the factor $e^{i\phi_j}$ in the RHS of eq. (5) by its ensemble average as

$$R = \sum_{\mathbf{r}'} G(\mathbf{r} - \mathbf{r}')\langle e^{i\phi}\rangle. \tag{11}$$

The average is the sum of the contributions from the coherent and incoherent groups, $\langle e^{i\phi}\rangle_{coh} = \int_{-\pi/2}^{\pi/2} \mathrm{d}\phi\, n(\phi) e^{i\phi}$ and $\langle e^{i\phi}\rangle_{incoh} = \int_{|\omega|>R} \mathrm{d}\omega P_\omega(\omega) \int_{-\pi}^{\pi} \mathrm{d}\phi n'(\phi;\omega) e^{i\phi}$. The latter vanishes because of the symmetry of $P_\omega(\omega)$, and the former with eq. (8) yields

$$R = RG_0 J(R), \tag{12}$$

$$J(R) = \int_{-\pi/2}^{\pi/2} \mathrm{d}\phi\, P_\omega(R\sin\phi)\cos^2\phi, \tag{13}$$

with $G_0 = \sum_{\mathbf{r}} G(\mathbf{r})$. This is a self-consistent equation for the mean-field amplitude. Expanding the integral as $J(R) = (\pi/2)[P_\omega(0) + P''_\omega(0)R^2/8 + O(R^4)]$, we obtain the critical coupling strength

$$G_{0c} = \frac{2}{\pi P_\omega(0)} \tag{14}$$

for the synchronization transition (at which a non-vanishing solution R appears). For a square lattice, we have $G_0 = 9.03 \cdot 3\gamma\omega_0/4\pi$. Also we have $P_\omega(0) = 1/(\sqrt{2\pi}\omega_0\delta_0)$. Putting these together into eq. (14), we obtain the critical angle

$$\delta_{0c} = 1.35\gamma. \tag{15}$$

In the simulation we used $\gamma = 0.1$, which gives $\delta_{0c} = 0.135$ (rad) $= 7.73$ (deg). This value is not very far from the numerically obtained threshold angle $\delta_{th} = 6$ (deg). In a real bacterial carpet, γ can be in the order of 10^{-2} as we estimated in the above. It means that a quite narrow distribution of the mounting angle (below 1°) is required to achieve coordinated motion. On the other hand, the mean-field theory predicts a sharp transition, in contrast to the gradual crossover observed in the simulation. Near δ_{0c}, the orientational order parameter decays as $S \propto \sqrt{\delta_{0c} - \delta_0}$, while the normalized frequency deviation linearly approaches to the desynchronized limit as $1 - Q \propto \delta_{0c} - \delta_0$. The distribution of the actual frequency $P_\Omega(\Omega)$ for $\delta_0 < \delta_{0c}$ has three distinct peaks, one at $\omega = 0$ (the coherent group) and two symmetric peaks for $\omega > 0$ and $\omega < 0$ (the incoherent group). The central peak vanishes for $\delta_0 > \delta_{0c}$. These behaviors are qualitatively different from the numerical results shown in figs. 2 and 3. In order to explain the unconventional transition behavior, it is necessary to develop a theoretical framework that incorporates spatial fluctuations, which is an interesting problem for the future.

Conclusion. – The synchronization transition caused by long-range hydrodynamic coupling is shown to be more gradual than for the global coupling. The threshold angle for the crossover is estimated, and is not far from the mean-field estimate for the transition point. It suggests that a very narrow angle distribution is required to achieve correlated motion in a real bacterial carpet. We believe that this work sheds some light on the delicate issues involved in hydrodynamic synchronization and hope that it stimulates further theoretical and experimental studies of the rich behavior of such systems.

* * *

NU thanks the hospitality at the University of Sheffield where this work was initiated, and financial support from Grant-in-Aid for Scientific Research from MEXT. RG acknowledges financial support from the EPSRC.

REFERENCES

[1] Kuramoto Y., *Chemical Oscillations Waves, and Turbulence* (Springer, New York) 1984.
[2] Acebrón J. A. *et al.*, *Rev. Mod. Phys.*, **77** (2005) 137.
[3] Crawford J. D. and Davies K. T. R., *Physica D*, **125** (1999) 1.
[4] Sakaguchi H., Shinomoto S. and Kuramoto Y., *Prog. Theor. Phys.*, **77** (1987) 1005.
[5] Kuramoto Y., *Prog. Theor. Phys.*, **94** (1995) 321; Kuramoto Y. and Battogtokh D., *Nonlinear Phenom. Complex Syst.*, **5** (2002) 380.
[6] Abrams D. M. and Strogatz S. H., *Phys. Rev. Lett.*, **93** (2004) 174102.
[7] Rogers J. L. and Wille L. T., *Phys. Rev. E*, **54** (1996) R2193.
[8] Maródi M., d'Ovidio F. and Vicsek T., *Phys. Rev. E*, **66** (2002) 011109.
[9] Tarasov V. E. and Zaslavsky G. M., *Chaos*, **16** (2006) 023110; Korabel N., Zaslavsky G. M. and Tarasov V. E., *Commun. Nonlinear Sci. Numer. Simul.*, **12** (2007) 1405.
[10] Taylor G. I., *Proc. R. Soc. A*, **209** (1951) 447.
[11] Riedel I. H., Kruse K. and Howard J., *Science*, **309** (2005) 300.
[12] Reichert M. and Stark H., *Eur. Phys. J. E*, **17** (2005) 493.
[13] Yang Y., Elgeti J. and Gompper G., *Phys. Rev. E*, **78** (2008) 061903.

[14] Goldstein R. E., Polin M. and Tuval I., *Phys. Rev. Lett.*, **103** (2009) 168103.
[15] Gueron S. and Levit-Gurevich K., *Proc. Natl. Acad. Sci. U.S.A.*, **96** (1999) 12240.
[16] Lagomarsino M. C., Bassetti B. and Jona P., *Eur. Phys. J. B*, **26** (2002) 8188; Lagomarsino M. C., Jona P. and Bassetti B., *Phys. Rev. E*, **68** (2003) 021908.
[17] Lenz P. and Ryskin A., *Phys. Biol.*, **3** (2006) 205; Niedermayer T., Eckhardt B. and Lenz P., *Chaos*, **18** (2008) 037128.
[18] Vilfan A. and Jülicher F., *Phys. Rev. Lett.*, **96** (2006) 058102.
[19] Guirao B. and Joanny J.-F., *Biophys. J.*, **92** (2007) 1900.
[20] Darnton N. *et al.*, *Biophys. J.*, **86** (2004) 1863.
[21] Kim M. J. and Breuer K. S., *ASME J. Fluid Eng.*, **129** (2007) 319; *Small*, **4** (2008) 111.
[22] Uchida N. and Golestanian R., preprint arXiv:0911.4253.
[23] Blake J. R., *Proc. Cambridge Philos. Soc.*, **70** (1971) 303.